A Numerical Investigation of Valve Timing and Intake Pressure Effects on Performance and Emissions in a Hydrogen Port Fuel Injection Engine

Isuru Wickramaarachchi[1, a *], Indrajith D. Nissanka[1,b] and Sameera Wijeyakulasuriya[2,c]

[1]Department of Mechanical Engineering, University of Moratuwa, Katubedda, Sri Lanka

[2]Convergent Science, Inc., 6400 Enterprise Lane, Madison, WI 53719, USA

[a]wickramaarachchiim.19@uom.lk, [b]nissankai@uom.lk, [c]sameera.wijeyakulasuriya@convergecfd.com

KEYWORDS: *Port Fuel; Valve Timing; Intake Pressure; Performance; Emissions*

ABSTRACT

Hydrogen internal combustion engines (H_2ICEs) offer a viable low-emission alternative for decarbonizing transport, especially where full electrification is not practical. Among fueling strategies, port fuel injection (PFI) is particularly attractive due to its compatibility with existing engine platforms and simplicity compared to direct injection (DI). Performance and emissions in hydrogen PFI engines are strongly influenced by valve timing and intake boosting strategies. This study presents a computational framework to investigate the coupled effects of valve timing and intake pressure on the performance, thermal efficiency, and NO_x emissions of a hydrogen PFI engine under fuel-lean conditions (ϕ = 0.59). A modified Sandia optical engine geometry was simulated using CONVERGE CFD v4.1, employing detailed chemistry and adaptive mesh refinement. Latin Hypercube Sampling (LHS) was employed to generate 373 design cases that span a wide parametric space. Results show that intake boosting significantly improves performance, achieving a 220% increase in indicated power (up to 43.55 kW) and an 11% improvement in thermal efficiency (up to 48.7%) over the baseline configuration. However, these gains are accompanied by elevated NO_x emissions, particularly at higher valve overlaps. Conversely, the configuration that achieved the lowest NO_x emissions reduced them by 76% compared to the baseline, albeit at the expense of lower power and efficiency. The three configurations representing the most favorable outcomes for power, efficiency, and emissions within the studied parameter space highlight the inherent trade-offs among these objectives. These results provide practical guidance for calibrating hydrogen PFI engines and establish a solid foundation for future studies incorporating formal optimization methods.

INTRODUCTION

The continued rise in global greenhouse gas (GHG) emissions poses a critical challenge for policymakers, industry stakeholders, and researchers worldwide. The Intergovernmental Panel on Climate Change (IPCC) has stressed in its Sixth Assessment Synthesis Report that achieving the 1.5°C target requires rapid and sustained reductions in CO_2 and other GHGs [1]. In 2024 alone, energy-related CO_2 emissions reached 37.4 GT, marking a 410 MT increase from the previous year [2]. The transportation sector remains a significant contributor, accounting for over a quarter of these emissions, primarily from light-duty internal combustion engine (ICE) vehicles [3]. Battery electric vehicles (BEVs) have emerged as the leading strategy for decarbonizing transport. However, their overall environmental impact is closely tied to the carbon intensity of electricity generation. With over 60% of global electricity still derived from fossil fuels in 2024, the actual emissions reduction from BEVs remains limited in many regions [2]. BEVs also face infrastructural, economic, and operational challenges, particularly in high-load or long-distance applications [4].

Hydrogen has gained attention as a complementary energy carrier capable of overcoming some of these limitations. It offers zero tailpipe emissions and high gravimetric energy density, making it suitable for sectors where electrification remains impractical. Hydrogen can be utilized in both fuel cell electric vehicles (FCEVs) and hydrogen-fuelled internal combustion engines (H_2ICEs). While FCEVs offer high efficiency and quick refueling [5], they are hindered by high system costs, durability concerns, and limited fueling infrastructure [6]. In contrast, H_2ICEs offer a cost-effective and technically mature pathway, especially for retrofitting existing vehicle fleets. Hydrogen's favorable combustion properties—including high flame speed, wide flammability range, and low ignition energy—enable lean operation and reliable cold starts. Moreover, H_2ICEs are compatible

https://doi.org/10.54389/JXFC7763

with existing ICE manufacturing and servicing ecosystems, allowing rapid deployment with minimal infrastructure changes [7]. Among fueling strategies, port fuel injection (PFI) and direct injection (DI) are commonly employed in hydrogen engines. While DI offers improved mixture control, it involves a higher cost and system complexity. PFI is simpler and more suitable for retrofitting gasoline engines. Recent studies indicate that hydrogen PFI engines can achieve high thermal efficiency and low emissions under ultra-lean conditions [8].

Within this context, two key engine parameters—valve timing and intake pressure—play crucial roles in controlling combustion behavior and emissions. Prior research has shown that both valve timing and intake boosting significantly influence hydrogen engine performance and emissions [9], [10], [11]. However, most existing studies are experimental and limited in parametric scope. High-fidelity CFD studies that investigate the coupled effects of valve timing and intake boosting under realistic operating conditions remain scarce. To address this gap, the present study develops a CFD-based computational framework to systematically explore the combined influence of valve timing and intake charge boosting in a hydrogen-fueled PFI engine. By capturing detailed in-cylinder phenomena, this work aims to identify configurations that improve performance, thermal efficiency, and emissions without relying on complex auxiliary systems such as water injection and EGR.

LITERATURE REVIEW

The Valve timing is a key determinant of combustion dynamics, engine performance, and emissions in hydrogen-fueled spark ignition engines. Park et al. [10] experimentally investigated intake and exhaust valve timing in a hydrogen PFI engine under high-load conditions. Their findings showed that moderately advanced intake valve opening (IVO) enhanced airflow and torque, while excessive advancement caused residual gas interference, diminishing performance. Retarded exhaust valve closing further reduced volumetric efficiency. This study underscored the need for optimal valve timing to enhance power output and thermal efficiency. Lee et al. [9] extended this understanding by demonstrating that retarding IVO to top dead center (TDC) enabled stable ultra-lean operation at $\phi = 0.2$ and achieved near-zero NO_x emissions. Although volumetric efficiency declined, performance was recovered using supercharging, achieving gasoline-equivalent power and thermal efficiency above 39%. This illustrated the synergistic potential of combining valve timing strategies with intake boosting. Huynh et al. [12] examined valve overlap time (VOT) variations from 0^0 to 50^0 CA and found that changes in overlap influenced mixture formation and combustion efficiency. While maximum torque was achieved around VOT = 30^0 CA, shorter overlaps still yielded satisfactory performance when energy input was adjusted. These findings collectively highlight the role of coordinated valve timing in optimizing engine output and reducing emissions under lean-burn conditions.

In parallel, intake boosting methods such as turbocharging and supercharging have proven effective in addressing the volumetric efficiency limitations inherent in hydrogen PFI engines. Jilakara et al. [13] experimentally evaluated a turbocharged, intercooled hydrogen engine designed for ultra-lean operation ($\phi = 0.5$–0.6) in a mini-bus application. Their setup delivered 66.7 kW at 3200 rpm while maintaining low combustion variability. However, turbo lag at low engine speeds remained a challenge. Verhelst et al. [14] explored supercharging options in a single-cylinder PFI engine and compared lean-burn and stoichiometric strategies. Lean supercharging ($\lambda \geq 2$) emerged as the more favorable approach, offering higher thermal efficiency and NO_x levels below 100 ppm across a broad speed range. The study also cautioned against increased NO_x formation at elevated pressures, which could be mitigated through EGR or leaner mixtures. Lee et al. [15] conducted a simulation-based analysis of turbocharged hydrogen engines and observed that moderate boost pressures improved power and airflow but also raised combustion temperatures, potentially increasing NO_x emissions under stoichiometric conditions. Nguyen et al. [16] corroborated these findings through experiments on a small-scale H_2ICE, confirming power enhancement from supercharging, while stressing the importance of spark timing optimization to maintain combustion efficiency.

Despite these contributions, existing studies typically focus on either valve timing or intake pressure in isolation, often within limited experimental setups. Few have examined their combined influence using high-resolution CFD approaches. As hydrogen PFI engines operate under complex, coupled thermochemical conditions, a comprehensive simulation-based exploration of valve timing and intake boosting interactions is essential. This study addresses that gap by providing a detailed CFD framework to inform future H_2ICE development.

NUMERICAL MODEL

The Due to the unavailability of a dedicated experimental research facility and the absence of a publicly available PFI engine geometry with sufficient experimental validation data, the single cylinder optically accessible DI hydrogen engine developed by Sandia National Laboratories [12] was selected as the baseline geometry for this study. The engine specifications and operating conditions are summarized in Table 1.

Table 1: Engine specifications and operating conditions

Description	**Value**
Bore	92 [mm]
Stroke	85 [mm]
Displacement	565 [cc]
Compression ratio	10.91
Engine speed	1500 [rpm]
Intake valve timing (IVO/IVC)	346/ -140 [CAD] aTDC
Exhaust valve timing (EVO/EVC)	130/ 346 [CAD] aTDC
Intake temperature	309 K

This engine geometry has been employed in numerous prior studies. Scarcelli et al. [13] developed a 3D CFD model to analyze hydrogen jet dynamics, showing that high mesh resolution near the injector is crucial for capturing jet penetration and stratification, with strong agreement to PLIF measurements. Barbato and Cantore [14] conducted full-cycle simulations and validated their adaptive mesh refinement strategy using experimental data, emphasizing the need for accurate time resolution during the injection phase. Wu et al. [15] employed CONVERGE to investigate hydrogen–air mixing under different in-cylinder flow conditions. The original engine geometry is available in CONVERGE [16] and is illustrated in Fig. 1. It consists of distinct intake and exhaust ports (Fig. 1a), a tumble plate integrated into the intake path to enhance in-cylinder motion (Fig. 1b), and a centrally located direct injector with a side-mounted spark plug on the cylinder head (Fig. 1c).

To facilitate the investigation of hydrogen PFI operation, the original DI geometry was modified. The key modifications included removing the direct injector, eliminating the tumble plate, and repositioning the spark plug to the center of the cylinder head. These changes are shown in Fig 2. The intake ports were retained to simulate the entry of a premixed hydrogen–air charge through conventional intake valves. Although these modifications substantially alter the original DI configuration, they are justified within the context of this numerical investigation, which focuses on analyzing relative trends in performance and emissions rather than predicting absolute values.

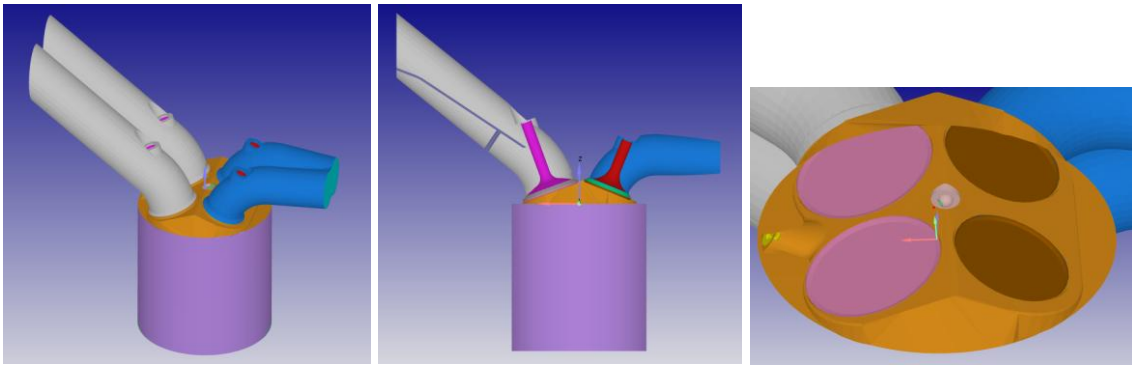

(a) (b) (c)

Figure 1: (a) Original Sandia DI engine geometry, (b) Cross-sectional view showing tumble plate, (c) Cylinder head showing DI injector and spark plug placement

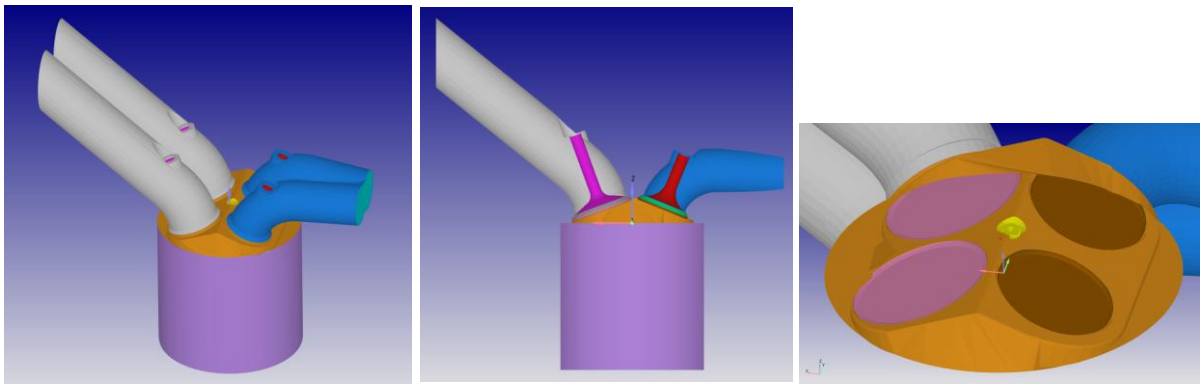

(a) (b) (c)

Figure 2: (a) Modified engine geometry for PFI operation, (b) Cross-sectional view without tumble plate, (c) Top view showing removed injector and repositioned spark plug

A fully premixed, homogeneous hydrogen–air mixture was assumed to enter the computational domain through the intake ports, consistent with a dry PFI system. To investigate the effects of valve timing on combustion dynamics, valve lift profiles were adapted to allow variation in VOT. Simulations were conducted using CONVERGE CFD v4.1, a state-of-the-art general-purpose CFD software. Each case was simulated over a full engine cycle, beginning at exhaust valve closing (EVC) and continuing through 720^0 crank angle rotations. To accurately capture flow and combustion phenomena, the computational mesh employed adaptive mesh refinement (AMR), which locally increased resolution in regions with steep velocity or temperature gradients, such as flame fronts and flow structures. Fixed embedding was also applied in key regions of interest, including the intake and exhaust valves and the spark plug, where ignition and mixing processes are critical. A grid independence study was performed using a base mesh size of 4 mm, with progressively increased AMR levels based on velocity and temperature criteria. Refinement level 2 was selected as it provided a good balance between accuracy and computational cost. Under these settings, the minimum cell size in the combustion zone was refined to 0.0625 mm during the ignition phase and 1 mm during flame propagation, with the overall cell count reaching a maximum of approximately 0.5 million during peak refinement.

The simulations solved the three-dimensional, transient, compressible Reynolds-Averaged Navier–Stokes (RANS) equations for conservation of mass, momentum, energy, and species transport within a finite volume framework. Turbulence was modeled using the Renormalization Group (RNG) k-ε turbulence model [17], which is well-suited for swirling and recirculating in-cylinder flows. The momentum, energy, and species transport equations were discretized using a second-order central difference scheme within a finite volume framework. Time integration was performed using a first-order implicit Euler scheme with a variable time-stepping algorithm to ensure numerical stability and efficiency across the engine cycle. Pressure–velocity coupling was handled via the PISO algorithm [18], while the gas density was computed based on the energy equation using the Redlich–Kwong real gas equation of state [19]. Wall heat transfer was modeled using the O'Rourke–Amsden model [20], applied to all solid regions. This model estimates instantaneous convective heat transfer coefficients based on in-cylinder conditions and wall geometry.

Turbulent scalar transport was modeled using a turbulent Schmidt number of 0.78 and a turbulent Prandtl number of 0.9. Combustion was simulated using the SAGE detailed chemistry solver [16], coupled with a hydrogen mechanism extracted from the C3MechV3.3 kinetic model [21]. This mechanism includes 12 species and 37 reactions and has been validated for ignition delays (600–2500 K, 0.65–40 atm, φ = 0.06–6) and laminar flame speeds (295–600 K, 1–10 atm, φ = 0.4–2.2). The SAGE solver uses the CVODE integrator from the SUNDIALS package [22] to solve the stiff system of ordinary differential equations governing the chemical kinetics. These equations are solved with internal time steps smaller than the main CFD time step, and the computed reaction source terms are passed to the species transport equations. Molecular diffusivities for each species were calculated using data from a dedicated transport file (transport.dat) [23]. Spark ignition was modeled via multiple staged energy deposition events to replicate spark kernel formation and early flame growth under realistic engine conditions [24]. All simulations were performed under globally lean conditions, with an equivalence ratio of $\varphi = 0.59$ ($\lambda \approx 1.7$). Spark timing was fixed across all cases to isolate the effects of VOT and intake pressure on combustion characteristics and emissions. Thermal NO_x formation was modeled using the extended Zeldovich mechanism [25] under the assumption of local thermodynamic equilibrium.

At the intake ports, total pressure was specified according to the target intake pressure condition for each case (ranging from atmospheric to 2.61325 bar), along with a total temperature of 309 K. At the exhaust ports, a fixed static pressure corresponding to atmospheric pressure was applied. All combustion chamber walls, piston crown,

and cylinder liner were modeled as no-slip boundaries with convective heat transfer calculated using the O'Rourke–Amsden model. The global equivalence ratio was fixed at φ = 0.59 for all cases, and spark timing was held constant to isolate the effects of VOT and intake pressure.

METHODOLOGY

Design of experiments

Latin hypercube sampling (LHS) [26] was employed to generate a statistically robust and space-filling design of experiments for this study. The sampling strategy focused on two key input parameters: VOT, which varied from 0^0 to 50^0 CA, and intake pressure, which ranged from 1.01325 to 2.61325 bar. Using this method, a total of 373 simulation cases were created, ensuring a comprehensive exploration of the design space. The distribution of the sample cases is illustrated in Fig. 3. Each case was simulated using the CFD setup described earlier. To isolate the effects of VOT and intake pressure, all other parameters including the global equivalence ratio ($\phi = 0.59$, $\lambda \approx 1.7$) and spark timing were held constant across the simulations. The simulations were executed on the CONVERGE Horizon cloud computing platform [27], with each case requiring approximately 5 hours on a 36-core machine. By running 10 machines in parallel, 10 simulations could be completed within 5 hours, enabling efficient execution of the full 373-case design space. This approach ensured the timely completion of the high-throughput CFD campaign while maintaining numerical consistency across all cases.

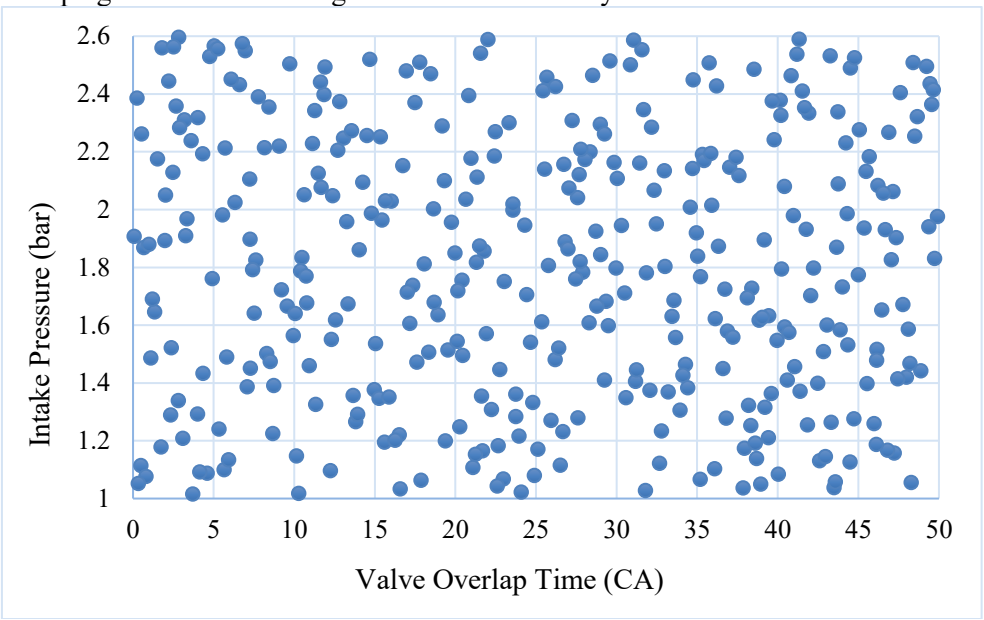

Figure 3: Latin Hypercube Sampling (LHS) distribution of 373 design points in the input parameter space

Performance and emission metrics

Each simulation output was post-processed to extract indicated power (kW), thermal efficiency (%), and NO_x Emissions (mg/cycle). These metrics were chosen to evaluate both engine performance and engine-out emissions.

RESULTS AND DISCUSSION

Effect of valve timing.

As shown in Fig. 4, increasing intake pressure results in a clear upward shift in indicated power across the entire VOT range. For each pressure level, power generally increases with VOT, although the rate of increase diminishes at higher overlaps. At an intake pressure of 2.6 bar, the engine reaches peak power levels exceeding 43 kW at VOT > 35^0 CA, while the power remains below 15 kW at atmospheric pressure, highlighting the dominant effect of intake boosting on volumetric efficiency and combustion energy release. Fig. 5 complements these findings by revealing corresponding trends in thermal efficiency. Efficiency increases with both intake pressure and VOT, particularly at mid-range overlaps (15–35^0 CA), where optimized intake-exhaust interaction and mixture quality contribute to better combustion. The highest thermal efficiency observed is approximately 48.7% at 2.6 bar, significantly outperforming lower intake pressure cases. Notably, while efficiency trends generally mirror power trends, the gains tend to plateau or even slightly decline beyond a certain VOT, suggesting diminishing benefits due to increased overlap-induced pumping losses or reduced volumetric efficiency at extreme settings.

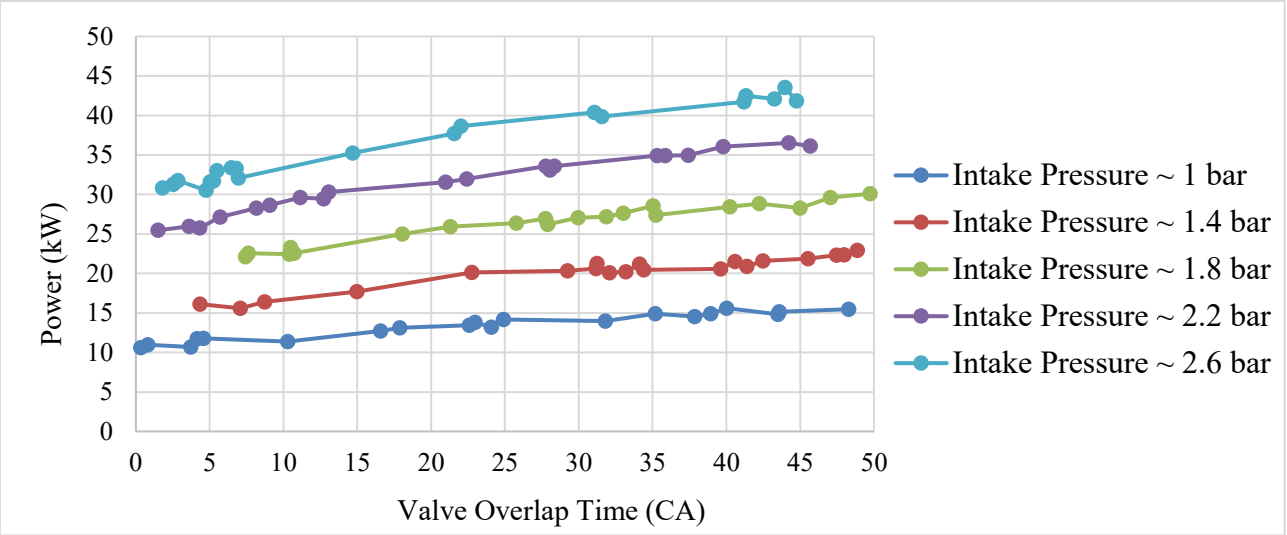

Figure 4: Effect of VOT on indicated power at various intake pressures

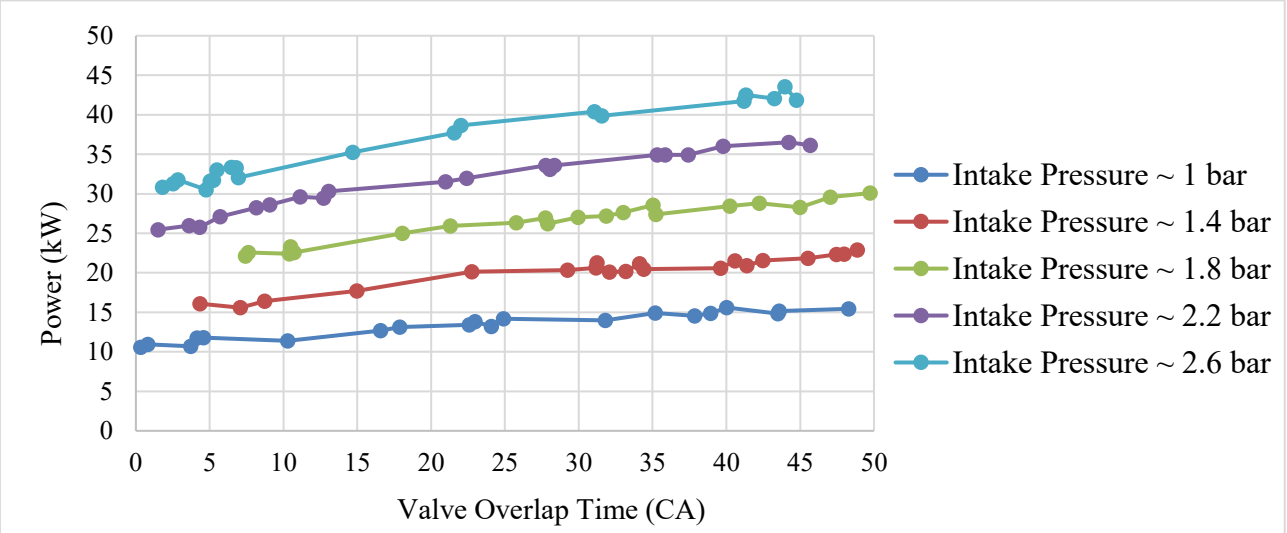

Figure 5: Effect of VOT on thermal efficiency at various intake pressures

Fig. 6 illustrates the variation of NO_x emissions, expressed as total NO_x mass per cycle, with VOT across five intake pressure levels ranging from approximately 1 bar to 2.6 bar. The results demonstrate that NO_x formation increases with both VOT and intake pressure, driven primarily by the elevated in-cylinder temperatures and oxygen availability associated with greater charge density and enhanced combustion intensity under boosted conditions. At low intake pressure (1–1.4 bar), NO_x emissions remain relatively modest and stable across the VOT range, suggesting limited peak temperature rise under lean conditions. However, as intake pressure increases to 2.2 and 2.6 bar, NO_x mass exhibits a pronounced upward trend with VOT, particularly beyond $20^0 – 25^0$ CA. This is attributed to longer valve overlaps promoting higher residual gas temperatures and more complete combustion, which intensify thermal NO_x generation. The highest NO_x values exceed 10 mg per cycle at 2.6 bar and high VOT, marking a significant emissions penalty associated with aggressive intake boosting and extended valve overlap.

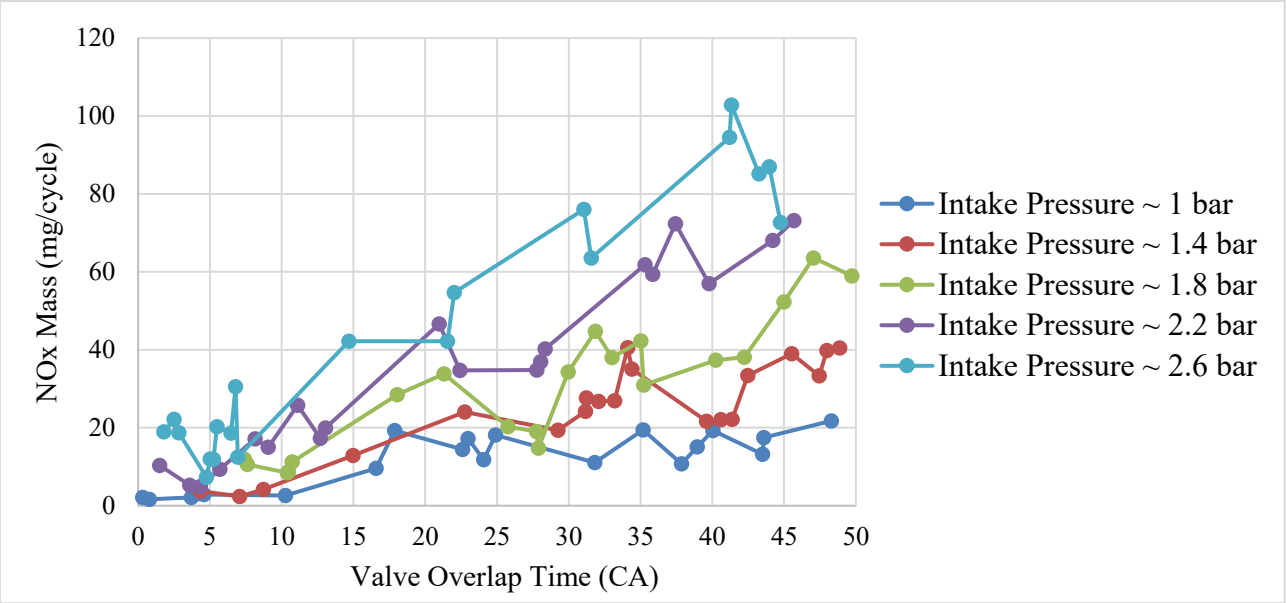

Figure 6: Effect of VOT on NO_x emissions at various intake pressures

Effect of intake pressure

Fig. 7 and 8 show the effect of intake pressure on indicated power and thermal efficiency. As intake pressure increases from 1.0 to 2.6 bar, both power output and thermal efficiency improve significantly due to higher charge density, enhanced volumetric efficiency, and more complete combustion. Intake boosting allows a greater mass of the hydrogen–air mixture to enter the cylinder, resulting in increased combustion energy and improved energy conversion. While power output shows a nearly linear increase with intake pressure, thermal efficiency gains tend to plateau at higher boost levels as secondary losses such as heat transfer and pumping work begin to offset further improvements.

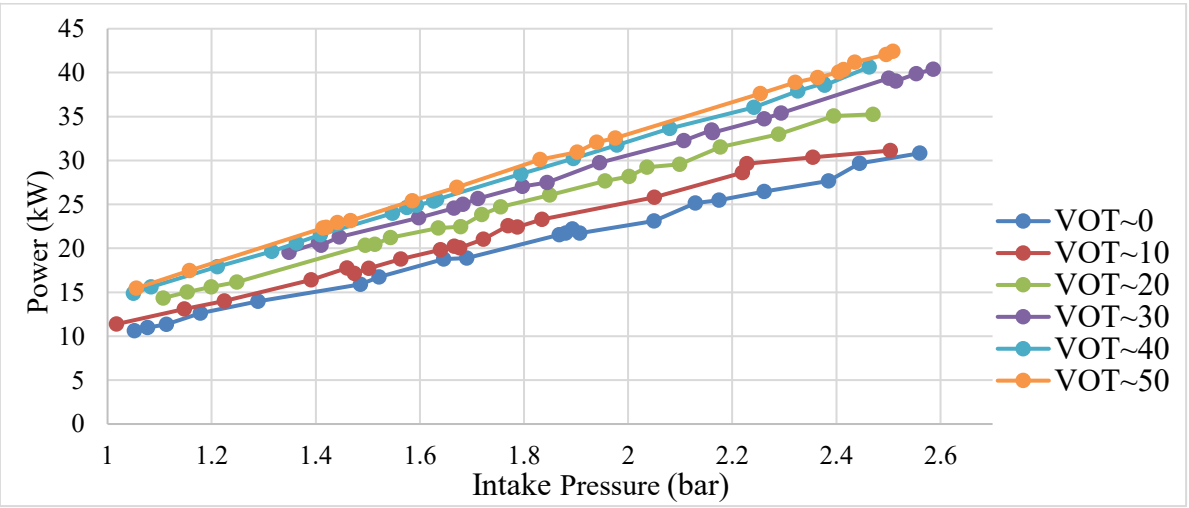

Figure 7: Effect of intake pressure on indicated power at various VOTs

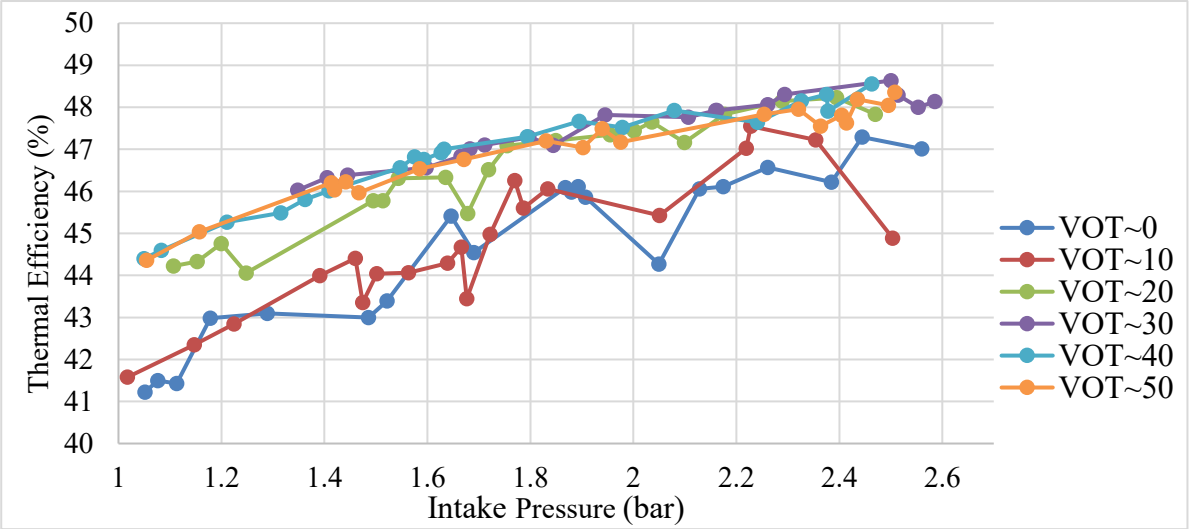

Figure 8: Effect of intake pressure on thermal efficiency at various VOTs

Fig. 9 illustrates the impact of intake pressure on NO_x emissions across various VOTs. As intake pressure increases from 1.0 to 2.6 bar, NO_x formation generally rises, with a more pronounced increase at higher VOT settings. This trend is attributed to elevated in-cylinder temperatures and oxygen availability under boosted conditions, which enhance thermal NO_x production. While low intake pressures result in minimal NO_x emissions regardless of VOT, higher pressures, especially above 2.0 bar, lead to a sharp rise in NO_x, particularly when combined with long valve overlaps.

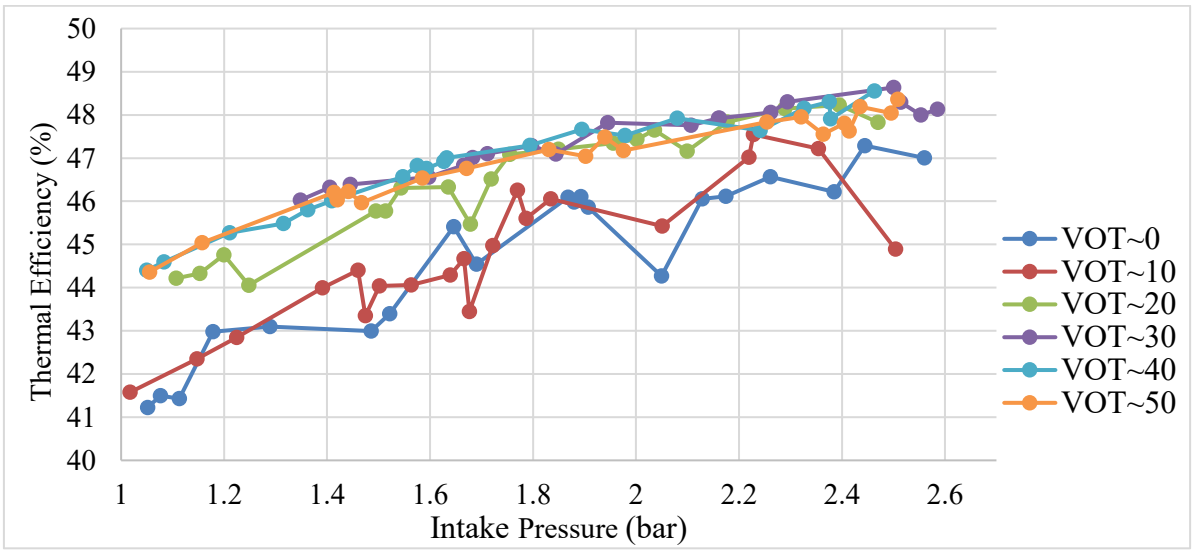

Figure 9: Effect of intake pressure on NO_x emissions at various VOTs

Best outcomes

Within the studied design space, three best operating points were identified, each corresponding to a different objective.

- Case A: Maximum power
- Case B: Maximum efficiency
- Case C: Minimum NO_x emissions

Table 2 presents the corresponding parameter combinations and highlights the trade-offs among power output, efficiency, and emissions. The baseline configuration is defined by a VOT of 30^0 and an intake pressure of 1.01325 bar. This case was selected as it represents a typical naturally aspirated setup and aligns with configurations previously identified as high performing for hydrogen PFI engines across a wide range of operating conditions [28]. Case A delivered the highest indicated power output of 43.55 kW, achieved at a VOT of 43^0 CA and an intake pressure of 2.61 bar. This represents a 221% increase in power compared to the baseline case, along with a thermal efficiency of 48.4%. However, this configuration resulted in elevated NO_x emissions of 8.69 mg per cycle. Case B yielded the maximum thermal efficiency of 48.7% at a VOT of 22^0 CA and an intake pressure of 2.59 bar. Compared to the baseline, this corresponds to an 11% improvement in efficiency and a substantial increase in power output to 38.66 kW, though with moderately high NO_x emissions of 5.47 mg per cycle. Case C

prioritized emissions reduction, achieving ultra-low NO_x emissions of just 0.17 mg per cycle, which marks a 76% reduction relative to the baseline. This was accomplished with a near-zero VOT of 0.8^0 CA and a near-atmospheric intake pressure of 1.08 bar. However, this strategy compromised performance, with power output reduced to 10.96 kW and thermal efficiency to 41.5%, illustrating the trade-off necessary to meet stringent emissions targets.

Table 2: Best parameter combinations for maximum power, thermal efficiency, and minimum NO_x emissions

Case	**VOT (CA)**	**Intake Pressure (bar)**	**Power (kW)**	**Efficiency (%)**	**NO_x (mg/cycle)**
Baseline	30.0	1.01325	13.54	43.9	0.72
A	43.0	2.61	43.55	48.4	8.69
B	22.0	2.59	38.66	48.7	5.47
C	0.8	1.08	10.96	41.5	0.17

CONCLUSION

This study developed and applied a detailed CFD-based framework to evaluate the effects of valve timing and intake pressure on combustion performance and NO_x emissions in a hydrogen port fuel injection engine operating under lean conditions. A total of 373 full engine cycle simulations were performed using Latin Hypercube Sampling to span a broad range of intake pressures and valve overlap timings. The results confirm that intake boosting plays a dominant role in enhancing engine performance. The configuration yielding maximum power achieved 43.55 kW, corresponding to a 220% increase over the baseline, while the most efficient case achieved a thermal efficiency of 48.7%, representing an 11% improvement. However, these benefits came with increased NO_x emissions, particularly at high intake pressures and extended valve overlaps. The configuration that achieved the lowest NO_x emissions reduced them by 76% compared to the baseline, although this came at the expense of power and efficiency. These findings highlight the inherent trade-offs between power, efficiency, and emissions in hydrogen port fuel injection engine design. The developed framework provides a solid basis for refining engine calibration and lays the groundwork for future integration of data-driven optimization and control strategies.

FUTURE WORK

Building on the CFD-based framework developed in this study, future work will focus on integrating machine learning (ML)-based surrogate modeling to enable faster and more adaptive engine optimization. Advanced regression techniques and ensemble learning methods will be trained on the existing simulation dataset to predict engine performance and emissions with significantly reduced computational cost. Furthermore, the framework will be extended to incorporate abnormal combustion phenomena, such as backfire and combustion instabilities, which are critical considerations for the practical deployment and calibration of hydrogen PFI engines.

ACKNOWLEDGEMENTS

The authors gratefully acknowledge Convergent Science for providing CONVERGE CFD software licenses and technical support. The authors also thank Convergent Science for granting access to the CONVERGE Horizon cloud computing platform, which enabled the high-throughput simulations required for this research.

REFERENCES

[1] K. Calvin et al., "IPCC, 2023: Climate Change 2023: Synthesis Report. Contribution of Working Groups I, II and III to the Sixth Assessment Report of the Intergovernmental Panel on Climate Change [Core Writing Team, H. Lee and J. Romero (eds.)]. IPCC, Geneva, Switzerland.," Intergovernmental Panel on Climate Change (IPCC), July 2023. doi: 10.59327/IPCC/AR6-9789291691647.

[2] IEA, "Global Energy Review 2025 – Analysis - IEA," IEA, Mar. 24, 2025. https://www.iea.org/reports/global-energy-review-2025

[3] IEA, "Global EV Outlook 2025 – Analysis - IEA," IEA, May 14, 2025. https://www.iea.org/reports/global-ev-outlook-2025

[4] M. K. Anser, S. Ali, M. Umair, R. Javid, and M. Tayab, "Optimizing hydrogen integration in vehicle fuel systems for sustainable development: A step towards economic decarbonization," Int. J. Hydrog. Energy, vol. 98, pp. 321–333, Jan. 2025, doi: 10.1016/j.ijhydene.2024.12.009.

[5] Z. Stępień, "A Comprehensive Overview of Hydrogen-Fueled Internal Combustion Engines: Achievements and

Future Challenges," Energies, vol. 14, no. 20, p. 6504, Oct. 2021, doi: 10.3390/en14206504.
[6] Y. He, Y. Zhou, Z. Wang, J. Liu, Z. Liu, and G. Zhang, "Quantification on fuel cell degradation and techno-economic analysis of a hydrogen-based grid-interactive residential energy sharing network with fuel-cell-powered vehicles," Appl. Energy, vol. 303, p. 117444, Dec. 2021, doi: 10.1016/j.apenergy.2021.117444.
[7] K. Naseem et al., "Essential parts of hydrogen economy: Hydrogen production, storage, transportation and application," Renew. Sustain. Energy Rev., vol. 210, p. 115196, Mar. 2025, doi: 10.1016/j.rser.2024.115196.
[8] A. H. Khalid et al., "Hydrogen port fuel injection: Review of fuel injection control strategies to mitigate backfire in internal combustion engine fuelled with hydrogen," Int. J. Hydrog. Energy, vol. 66, pp. 571–581, May 2024, doi: 10.1016/j.ijhydene.2024.04.087.
[9] J. Lee, K. Lee, J. Lee, and B. Anh, "High power performance with zero NOx emission in a hydrogen-fueled spark ignition engine by valve timing and lean boosting," Fuel, vol. 128, pp. 381–389, July 2014, doi: 10.1016/j.fuel.2014.03.010.
[10] C. Park, W. Park, Y. Kim, Y. Choi, and B. Lim, "Effect of Valve Timing and Excess Air Ratio on Torque in Hydrogen-Fueled Internal Combustion Engine for UAV," Energies, vol. 12, no. 5, p. 771, Feb. 2019, doi: 10.3390/en12050771.
[11] S. Verhelst, P. Maesschalck, N. Rombaut, and R. Sierens, "Increasing the power output of hydrogen internal combustion engines by means of supercharging and exhaust gas recirculation," Int. J. Hydrog. Energy, vol. 34, no. 10, pp. 4406–4412, May 2009, doi: 10.1016/j.ijhydene.2009.03.037.
[12] "Hydrogen Engine," Engine Combustion Network. Accessed: June 12, 2025. [Online]. Available: https://ecn.sandia.gov/engines/hydrogen-engine/
[13] R. Scarcelli, T. Wallner, N. Matthias, V. Salazar, and S. Kaiser, "Numerical and Optical Evolution of Gaseous Jets in Direct Injection Hydrogen Engines," presented at the SAE 2011 World Congress & Exhibition, Apr. 2011, pp. 2011-01–0675. doi: 10.4271/2011-01-0675.
[14] A. Barbato and G. Cantore, "3D CFD simulation of a gaseous fuel injection in a hydrogen-fueled internal combustion engine," E3S Web Conf., vol. 312, p. 07001, 2021, doi: 10.1051/e3sconf/202131207001.
[15] B. Wu, R. Torelli, and Y. Pei, "Numerical modeling of hydrogen mixing in a direct-injection engine fueled with gaseous hydrogen," Fuel, vol. 341, p. 127725, June 2023, doi: 10.1016/j.fuel.2023.127725.
[16] Richards, K. J., Senecal, P. K., and Pomraning, E., CONVERGE 4, Convergent Science, Madison, WI (2024).
[17] V. Yakhot and S. A. Orszag, "Renormalization group analysis of turbulence. I. Basic theory," J. Sci. Comput., vol. 1, no. 1, pp. 3–51, 1986, doi: 10.1007/BF01061452.
[18] R. I. Issa, "Solution of the implicitly discretised fluid flow equations by operator-splitting," J. Comput. Phys., vol. 62, no. 1, pp. 40–65, Jan. 1986, doi: 10.1016/0021-9991(86)90099-9.
[19] Otto. Redlich and J. N. S. Kwong, "On the Thermodynamics of Solutions. V. An Equation of State. Fugacities of Gaseous Solutions.," Chem. Rev., vol. 44, no. 1, pp. 233–244, Feb. 1949, doi: 10.1021/cr60137a013.
[20] A. A. Amsden, P. J. O'Rourke, and T. D. Butler, "KIVA-II: A computer program for chemically reactive flows with sprays," LA-11560-MS, 6228444, May 1989. doi: 10.2172/6228444.
[21] S. Dong et al., "A new detailed kinetic model for surrogate fuels: C3MechV3.3," Appl. Energy Combust. Sci., vol. 9, p. 100043, Mar. 2022, doi: 10.1016/j.jaecs.2021.100043.
[22] "SUNDIALS | Computing." Accessed: June 18, 2025. [Online]. Available: https://computing.llnl.gov/projects/sundials
[23] T. Coffee and J. Heimerl, "Transport algorithms for premixed, laminar steady-state flames," Combust. Flame, vol. 43, pp. 273–289, 1981, doi: 10.1016/0010-2180(81)90027-4.
[24] J. B. Heywood, Internal combustion engine fundamentals. in McGraw-Hill series in mechanical engineering. New York: McGraw-Hill, 1988.
[25] G. A. Lavoie, J. B. Heywood, and J. C. Keck, "Experimental and Theoretical Study of Nitric Oxide Formation in Internal Combustion Engines," Combust. Sci. Technol., vol. 1, no. 4, pp. 313–326, Feb. 1970, doi: 10.1080/00102206908952211.
[26] M. D. McKay, R. J. Beckman, and W. J. Conover, "A Comparison of Three Methods for Selecting Values of Input Variables in the Analysis of Output from a Computer Code," Technometrics, vol. 21, no. 2, p. 239, May 1979, doi: 10.2307/1268522.
[27] "CONVERGE Horizon," Convergecfd.com, 2025. https://convergecfd.com/products/horizon (accessed Aug. 16, 2025).
[28] T. C. Huynh, J. K. Kang, K. C. Noh, J. T. Lee, and J. A. Caton, "Controlling Backfire Using Changes of the Valve Overlap Period for a Hydrogen-Fueled Engine Using an External Mixture," in ASME 2007 Internal Combustion Engine Division Fall Technical Conference, Charleston, South Carolina, USA: ASMEDC, Jan. 2007, pp. 243–251. doi: 10.1115/ICEF2007-1702.